Impact of the Enfuvirtide Resistance Mutation N43D and the Associated Baseline Polymorphism E137K on Peptide Sensitivity and Six-Helix Bundle Structure[†,‡]

Xuefang Bai,[§] Karen L. Wilson,[§] Jennifer E. Seedorff,[§] Douglas Ahrens,[§] Justin Green,[§] Donna K. Davison,[||] Lei Jin,[||] Sherry A. Stanfield-Oakley,[||] Sarah M. Mosier,[||] Thomas E. Melby,[||] Nick Cammack,[⊥] Zhongmin Wang,[@] Michael L. Greenberg,[||] and John J. Dwyer*[,§]

Protein Engineering Group and Virology Group, Trimeris, Inc., 3500 Paramount Parkway, Morrisville, North Carolina 27560, Roche, Palo Alto, California 94304, and ZM Consulting, Madison, Alabama 35758

Received December 21, 2007; Revised Manuscript Received May 1, 2008

ABSTRACT: Enfuvirtide (ENF), the first human immunodeficiency virus type 1 (HIV-1) fusion inhibitor approved for clinical use, acts by binding to gp41 heptad repeat 1 (HR1) and preventing its interaction with the viral HR2 region. Treatment-emergent resistance to ENF has been mapped to residues within HR1, and these mutations decrease its susceptibility to ENF and may reduce viral fitness and pathogenesis, although the mechanism for these effects is not clear. N43D, a common ENF resistance mutation, was found in in vitro assays to cause a 5−50-fold in antiviral activity. We introduced this mutation into peptide models and determined the impact of this mutation by circular dichroism and X-ray crystallography. We find that the mutation results in a decrease in the thermal stability of the six-helix bundle and causes a significant change in the HR1−HR2 interface, including a loss of HR2 helicity. These data form a mechanistic basis for the decrease in ENF sensitivity and six-helix bundle stability. The E137K polymorphism, generally present at baseline in patients who develop N43D, partially compensates for the loss of stability, and we show that these residues likely form an ion pair. These data form a framework for understanding the impact of resistance mutations on viral fitness and pathogenesis and provide a pathway for the development of novel fusion inhibitor peptides.

Enfuvirtide (ENF),[1] the first fusion inhibitor (FI) approved for the treatment of human immunodeficiency virus (HIV), is a 36-amino acid peptide that acts by binding to the heptad repeat 1 (HR1) region of gp41 (*1, 2*) and preventing the interaction of the HR1 and heptad repeat 2 (HR2) domains, which is required for viral fusion. In the current model of HIV fusion, viral glycoproteins interact with CD4 and coreceptors on the target cell, leading to a large conformational change in gp120. This rearrangement results in the insertion of the fusion peptide of gp41 into the cellular membrane of the target cell. At this fusion intermediate step, the HR1 and HR2 domains of gp41 are exposed and eventually interact to form the trimer of hairpins (also known as the six-helix bundle). It is thought that the formation of this bundle brings the viral and cellular membranes together to facilitate fusion. ENF and other HR2 peptides are thought to bind to the trimeric HR1 domain during this fusion intermediate step and prevent the formation of the six-helix bundle.

Resistance to ENF has been observed both in vitro (*3, 4*) and during clinical studies (*5–8*). Many of these resistance mutations were localized to amino acids 36−45 on HR1, and these mutations have been generally shown to reduce the level of ENF binding and sensitivity in vitro (*5, 9, 10*). The mechanism by which ENF sensitivity is reduced is thought to be a decrease in the affinity of the peptide for mutated, viral HR1 (*3, 10*). However, these mutations are also likely to impact the interaction between the viral HR1 and HR2 domains, and this decrease in viral bundle stability may alter fusion kinetics, pathogenicity, replicative fitness, immunological recognition, and other aspects of the viral fusion process (*11, 12*). Furthermore, it has been shown recently that V38A (*13, 14*) and, to a lesser extent, N43D (*14*) are associated with sustained increases in CD4+ cell counts in patients who have developed resistance to ENF. As the mechanism for this immunological benefit is unclear, there is a great need to understand how resistance mutations alter the structure and function of gp41.

In the T-20 versus Optimized Regimen Only (TORO) phase III clinical trials of ENF, N43D was one of the most common treatment-acquired mutations (*6, 8, 15*). Among those patients reaching virologic failure, as many as 30% were found to have a mutation at position 43, with Asp-43 being the most frequent (*6, 8*). This mutation is also associated with decreased sensitivity to ENF. Primary isolates

[†] Financial support of this work by Roche is gratefully acknowledged.

[‡] The coordinates of the N34LC28/N43D, N45LC36/N43D, and N45LC36/N43D/E137K mutants have been deposited in the Protein Data Bank as entries 2OT5, 3CP1, and 3CYO, respectively.

* To whom correspondence should be addressed: Virology Group, Trimeris Inc., 3500 Paramount Pkwy., Morrisville, NC 27560. Phone: (919) 419-6050. Fax: (919) 408-5191.

[§] Protein Engineering Group, Trimeris, Inc.

[||] Protein Engineering Group, Trimeris, Inc.

[⊥] Roche.

[@] ZM Consulting.

[1] Abbreviations: HIV, human immunodeficiency virus; HR1 and HR2, heptad repeat regions 1 and 2, respectively, of HIV gp41; ENF, enfuvirtide (also known as Fuzeon and T-20); FI, fusion inhibitor; TORO, T-20 versus Optimized Regimen Only.

10.1021/bi702509d CCC: $40.75
Published on Web 05/29/2008

from patients who acquired the N43D mutation are 123−249-fold less sensitive to ENF than baseline isolates from the same patients (*6, 10*). Site-directed mutagenesis of N43D into laboratory-adapted strains shows a decrease in ENF susceptibility of 18−23-fold (*5, 10*). These data support the hypothesis that the primary mechanism for increased viral loads is the decrease in ENF sensitivity associated with these mutations.

Although viruses containing resistance mutations are capable of replicating in the presence of ENF, it has been shown that for many of these mutations, replicative fitness in the absence of ENF is reduced relative to that of the parental strain. This idea is supported by observed reductions in replicative fitness in cases where ENF resistance mutations were engineered into the virus by site-directed mutagenesis. These data showed that single mutations resulted in a decrease in fitness and that this decrease was generally proportional to the loss of ENF sensitivity (*11*). Furthermore, double mutations were shown to be significantly less fit than single mutations, suggesting that multiple substitutions in gp41 may be more deleterious to the virus (*11*) and certain mutations within amino acids 36−45 appear to be mutually exclusive (*11, 16*). Decreased viral fitness is also evident in the clinical setting, where discontinuation of ENF upon viral failure results in a rapid re-emergence of ENF-sensitive strains (*7, 15, 17*). Furthermore, it has been shown that N43D decreases infectivity 92% compared to that of the wild type, demonstrating that this mutation also results in a fitness defect (*18*).

Recently, it has been shown that these fitness defects may extend to viral pathogenicity. In a study of 54 ENF-treated patients, it was found that mutations at position 38 (specifically, V38A and V38E) were associated with a 4−6-fold increase in CD4+ cell counts despite viral failure (*13*). In an analysis of the TORO clinical trial data, V38A and N43D were associated with persistent immunological benefits after viral load rebound (*14*). In contrast, the Q40H mutation was shown to be associated with the loss of CD4+ cells, which is expected with viral load rebound (*13, 14*). Therefore, V38A and N43D appear to impact pathogenicity in a way that is distinct from at least some other mutations at positions 36−45 on gp41.

Alterations in fitness and pathogenesis may be related to the structural impact of these mutations on gp41. Mutations in HR1 of gp41 can be very deleterious to envelope processing and viral fusion (*19–23*), and this structural sensitivity is likely reflected in the high degree of sequence conservation observed in the HR1 region. Asn-43 participates in a conserved network of hydrogen bond interactions between HR1 and HR2 that has been termed the "glutamine-rich layer" (*24, 25*). A few studies have looked at the impact of specific changes in the glutamine-rich layer of the six-helix bundle (*19, 23*), but the functional role of this region remains unclear.

The negative impact of resistance mutations within gp41 on viral function may also lead to the appearance of secondary mutations that act to compensate for these defects. Analysis of the TORO data identified HR2 mutations that were associated with the appearance of an HR1 mutation (*8*). One such case, S138A, has been studied in some detail (*15*). In this work, we show that the N43D mutation appears almost exclusively with the natural baseline polymorphism E137K during the TORO clinical trials, suggesting that position 137 within HR2 has influence over mutations at position 43. Although the loss of enfuvirtide activity in response to resistance is likely due to a decrease in the binding affinity of the peptide for HR1, the details of how N43D, and the potential compensatory changes due to E137K, alter the structure of the six-helix bundle have not been elucidated. Furthermore, the fitness costs associated with resistance mutations suggest that more robust fusion inhibitors may exhibit a higher genetic barrier to resistance and be more potent against ENF-resistant viruses (*26*).

Here, we report the high-resolution crystallographic structure of six-helix bundles containing N43D (N554D in gp160 nomenclature), to assess how this change alters the binding interface between HR1 and HR2. In N34LC28, an HR1−HR2 chimera used previously for structural studies of the six-helix bundle (*24*), Asp-43 decreases bundle stability and is shown to significantly disrupt the hydrogen bonds formed between HR1 and HR2 in the glutamine-rich layer. The negative charge introduced by N43D also creates an unfavorable charge−charge interaction with Glu-137. These changes cause a loss of helical structure in the C-terminal end of the HR2 peptide. To the best of our knowledge, this is the largest structural change induced by a single mutation that has been observed in the six-helix bundle and demonstrates that resistance mutations can significantly alter the interaction between an HR2 peptide and the HR1 target. Interestingly, when the N43D mutation was introduced into a longer HR1−HR2 chimera (N45LC36), the structural impact was found to be significantly smaller.

We also show that the E137K (E648K) substitution partially compensates for the loss of bundle stability but does not repair all of the structural damage caused by N43D. By measuring the structural stability of these mutants at acidic pH, where Asp-43 should be uncharged, we show that E137K likely forms an ion pair with Asp-43 at pH 7. The structure of the N43D/E137K double mutant was determined in the N45LC36 construct and is consistent with the hypothesis that these residues are forming an ion pair.

This work provides a more detailed understanding of the mechanism by which resistance mutations decrease sensitivity to FI peptides and alter six-helix bundle structure. These data also provide an initial structural framework for interpreting how resistance mutations impact viral fitness and pathogenesis.

MATERIALS AND METHODS

Peptide Synthesis. Peptides were synthesized on a Rainin Symphony multiplex peptide synthesizer using 9-fluorenylmethoxycarbonyl (FMOC) chemistry protocols. Rink Amide MBHA resin was used for C-terminal amides and acetylated on the N-terminus using acetic anhydride and NMM in DMF so that each end was blocked. They were purified to >90% purity, and the peptide identity was confirmed by mass spectrometry.

Expression and Purification of HR1−HR2 Chimeras. A DNA fragment encoding the N34LC28 peptide was constructed by recombinant PCR and cloned into the pET41a vector (Novagen) at NdeI and XhoI sites. N45LC36 is composed of HR1 residues 536−579 and HR2 residues 628−663 from the IIIB strain of HIV. The two sequences

are connected by the SGGRGG linker. N43D and E137K mutations were introduced by site-directed mutagenesis. All constructs were transformed into BL21(DE3)pLysS competent cells (Novagen) for expression. Cells were induced with 1.0 mM IPTG for 4 h at 37 °C. Cell pellets were resuspended in 0.1 M NaOAc (pH 5) and 50 mM NaCl and lysed with a microfluidizer. N34LC28 cleared cell lysates were subjected to an S-column on an FPLC system, and fractions with chimeras of interest were pooled and purified to homogeneity by reverse phase HPLC, using a C18 column and a linear gradient of acetonitrile containing 0.1% TFA. N45LC36 lysates were initially purified using a Q-column on an FPLC system, and pooled fractions were purified to homogeneity using a column packed with phenyl Sepharose and a linear NaCl gradient. The purified chimeras were lyophilized, and their identities were confirmed by mass spectrometry.

Antiviral Activity. An NL4-3-based replication-competent virus containing a D36G substitution, GIV, was used as a template for site-directed mutagenesis (SDM), and ENF sensitivities were determined using a cMAGI infectivity assay (*27, 28*). Peptides were resuspended at ~1 mg/mL in PBS and serially diluted to final concentrations. The assay is based on a single cycle of infection. To ensure that secondary rounds of infection do not complicate the analysis, an active HR2 peptide (such as T-20 or T-1249) is added at high concentration to all wells 24 h postinfection. Seventy-two hours postinfection, cells are fixed with formaldehyde and glutaraldehyde and stained with X-Gal (5-bromo-4-chloro-3-indoyl β-D-galactopyranoside). Infected nuclei are counted using a charge-coupled device (CCD) detector. The IC_{50} is determined by interpolating the concentration required to inhibit viral replication by 50%.

For pseudotype assays, HIV-1 env genes from a patient-derived primary isolate, 030, and the GIV laboratory strain were cloned into an expression vector and served as a starting point for mutagenesis. Sensitivities to inhibition by ENF were determined with env-deficient reporter viruses pseudotyped with either the parental env or the env with the appropriate SDM.

Circular Dichroism. Lyophilized peptides were resuspended in phosphate buffer (pH 7) at approximately 1 mg/mL. Concentrations were determined using the method of Edelhoch (*29*). The percent helix was calculated from baseline-corrected wavelength scans using single-value decomposition with a basis set of 33 protein structures (*30*). Wavelength scans were collected at 25 °C on peptide solutions (1 or 10 μM) from 200 to 260 nm in 0.5 nm steps with a 4 s averaging time on an AVIV 202-01 circular dichroism spectrophotometer. Thermal unfolding of HR1−HR2 bundles was assessed at 222 nm with 2 °C increments from 25 to 97 °C with an averaging time of 16 s. T_m values for HR1−HR2 complexes were obtained by combining equal concentrations of each peptide and diluting the mixture to the appropriate concentration using PBS or PBS with 8 M urea. The T_m was determined to be the value that corresponded to the maximum value of the first derivative of the thermal transition (*31*).

Crystallization, Data Collection, and Structure Determination. Crystals were grown by the hanging drop vapor diffusion method at 25 °C. To grow crystals, a 30 mg/mL purified peptide stock in H_2O was diluted 1:1 with reservoir solution and allowed to equilibrate against the reservoir.

Table 1: Antiviral Activity of ENF against the Wild Type and Viruses Containing ENF Resistance Mutations

	cMAGI assay		pseudotype assay			
	GIV		GIV		030	
virus	IC_{50} (μg/mL)	*x*-fold change	IC_{50} (μg/mL)	*x*-fold change	IC_{50} (μg/mL)	*x*-fold change
WT	0.009	1	0.091	1	3.385	1
N43D	0.520	58	0.639	6.9	13.812	4.1
E137K	0.005	0.6	0.291	3.2	2.091	0.6
N43D/E137K	0.492	55.45	1.679	18.0	19.812	5.9

Initial crystallization conditions were screened by using sparse matrix crystallization kits (Crystal Screen I and II, Hampton Research) and then optimized. High-quality crystals of N34LC28 N43D were grown from 10% glycerol, 0.2 M $(NH_4)_2SO_4$, 23% PEG 4000, 50 mM NaOAc (pH 4.3), and 50 mM NaOAc (pH 4.6). Crystals of N45LC36 were grown in 25−40% ethylene glycol, 0.2 M $MgCl_2$, and 0.1 M HEPES (pH 7−8) in Cryschem plates (Charles Supper Co., Natick, MA). Data were collected on a Rigaku RU200 rotating anode X-ray generator, and the structures were determined by molecular replacement using CNX (Accelrys) and Protein Data Bank (PDB) entry 1STZ (*24*) or 1ENV (*32*) as an initial model. The coordinates of the N43D structure in both N34LC28 and N45LC36 as well as the double mutant, N43D/E137K, in N45LC36 have been deposited in the PDB (entries 2OT5, 3CP1, and 3CYO, respectively).

RESULTS

The N43D Resistance Mutation Leads to Decreased ENF Sensitivity. Amino acid substitutions within the region of amino acids 36−45 of gp41 (GIVQQQNNLL) have been shown to reduce the potency of ENF (*5, 9*) and decrease the level of binding of ENF to peptide targets (*10*). Table 1 shows the impact of N43D on the ENF sensitivity in two different assay systems. Site-directed mutagenesis of N43D into a laboratory-adapted NL4-3 strain (GIV) resulted in a 7−39-fold reduction in ENF sensitivity, depending on the assay that was used. An N43D mutation engineered into the 030 primary isolate resulted in a 4-fold decrease in sensitivity. These data are consistent with previously published data on these mutations in a variety of experimental systems (*6, 10, 18*).

At Virologic Failure, N43D Preferentially Emerged in Strains with an E137K Polymorphism at Baseline. Although the N43D mutation often occurred without any additional changes in the viral HR1, an association was observed between Asp-43 and position 137 in the HR2 region. Figure 1 shows that at baseline, position 137 is polymorphic and that patients who acquired N43D at virologic failure were much more likely to have Lys-137 at baseline than the overall population [72% vs 10%; $P < 0.0001$ (Fisher's exact test)]. At virologic failure, Lys-137 was still present and had emerged on treatment in three of 22 additional patients with N43D versus 4 of 265 without N43D ($P < 0.05$). Thus, patients with N43D had a much higher prevalence of Lys-137 at baseline than other patients and also experienced more frequent emergence of Lys-137 during therapy, strongly suggesting that Lys-137 offers an advantage to viruses containing N43D. Figure 2 shows the sequence overlap of the HR1 and HR2 regions in gp41 and shows that position 137 is directly adjacent to amino acid 43 in the six-helix

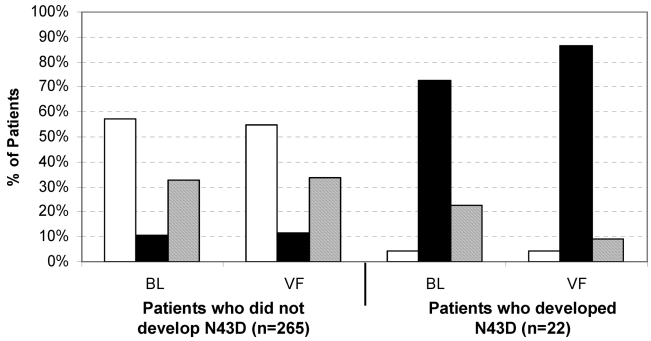

FIGURE 1: Distribution of genotypes at position 137 of the HIV gp41 envelope at baseline and virologic failure. Patients were subgrouped on the basis of the presence or absence of N43D at the time of failure. The percentage of patients with glutamic acid (white bars), lysine (black bars), or other amino acids or mixtures (including E137E/K) (hatched) at position 137 is shown at baseline and at virologic failure.

bundle. This raised the possibility that Asp-43 was directly interacting with Lys-137.

Table 1 reports the ENF sensitivity for viruses with the E137K substitution. Although E137K exhibited a 3-fold decrease in sensitivity in the GIV strain using the pseudotype assay, there was no decrease in the sensitivity of this strain in the cMAGI assay. The introduction of this substitution into the 030 primary isolate also showed no change in susceptibility. The ENF susceptibility of the N43D/E137K double mutant is also similar to that of N43D alone (Table 1), suggesting that E137K has little direct impact on ENF activity either alone or in combination with N43D.

Resistance Mutations Decrease Six-Helix Bundle Stability. To determine the impact of N43D and E137K on bundle stability, we analyzed HR1−HR2 complexes by circular dichroism (CD) (Table 2). Previously, we have looked at HR2 binding to a 51-amino acid HR1 peptide known as T-865 (*31*); however, this HR1 is not a good binding partner for ENF due to poor sequence overlap (Figure 2). HR1 peptide T-1847 was chosen for this work since it is a better binding partner for ENF and was previously shown to be monomeric (and not aggregated) over a wide range of concentrations (*31*). A synthetic T-1847 analogue with the N43D substitution was created, along with an ENF analogue containing the E137K substitution. A wavelength scan was used to determine the helical content of each peptide individually as well as the mixture of the HR1 and HR2. Table 2 shows that when ENF is mixed with T-1847, the helicity of the complex is 90%, as compared to 14% for the sum of the two individual peptides. An observed increase in the helicity of the mixture is indicative of an interaction between HR1 and HR2, which induces helical structure. When the N43D substitution is present, the helicity of the complex is only 26%, suggesting that ENF binds very weakly to mutated HR1 at pH 7. These data imply that ENF is not likely to bind the viral HR1 with high affinity. Unfortunately, the mixture of T-1847 with the ENF analogue E137K precipitated immediately upon mixing under these conditions (Table 3).

To further assess the impact on stability, thermal unfolding experiments were conducted with the HR1−HR2 complexes. At pH 7, the midpoint of the thermal melting transition, or T_m, is 47 °C for the T-1847−ENF complex, but when N43D is present in HR1, there is no detectable transition. The helicity and T_m data both support the notion that the HR1−ENF complex is significantly destabilized when N43D is present.

Since the HR1−ENF complexes have intrinsically low stability, and since we had precipitation issues with one of the complexes (see Table 2), we also introduced the N43D substitution into T-865 and into the chimeric HR1−HR2 construct, N34LC28 (*24*). For T-865, we used the HR2 peptide T-651, which has previously been shown to form a stable bundle with this HR1 (*26*). At pH 7, N43D reduced the bundle stability from 86 to 73 °C, which is close to the stability of HR1 alone. To eliminate the complication of the HR1 T_m, bundles were also melted in 8 M urea, a condition where HR1 is unable to form an oligomer in the absence of HR2. The thermal transitions of the wild-type (WT) and mutant bundles are shown in Figure 3, and the T_m values obtained are listed in Table 2. Under these conditions, N43D was found to decrease bundle stability by 24 °C, further demonstrating that this mutation has a deleterious impact on bundle stability.

E137K Partially Restores the Stability Lost by N43D. As shown in Table 2, the E137K substitution alone, either in peptide models using T-865 or in the N34LC28 chimera, has little to no effect on bundle stability (an increase of 1−2 °C). However, when N43D is present in HR1, E137K increases the stability of the bundle by as much as 9 °C (Table 2 and Figure 3). In the case of the N34LC28 construct, the N43D/E137K double mutant completely restores bundle stability to that of the WT. Even in the peptide models involving ENF, a complex is formed in the double mutant (with a T_m of 33 °C), whereas there is no apparent interaction with N43D alone. These data demonstrate that the impact of N43D on the stability of the bundle can be ameliorated by the presence of E137K and support the notion that these two residues may interact to form an ion pair.

The Interaction between N43D and E137K Is pH-Dependent. To test the hypothesis that Asp-43 and Lys-137 were forming an ion pair, we repeated the CD thermal melting experiments at pH 3. This pH is below the intrinsic pK_a of aspartic acid, so the side chain should exist in the uncharged (protonated) state. In contrast to the data at pH 7, the N43D substitution has little impact on either helicity or bundle stability at pH 3 (Table 2). The T_m values of the single mutants or the double mutant were all within 3−6 °C, suggesting that N43D no longer has a detrimental impact on stability and that E137K no longer contributes to the stability of the complex in the presence of N43D.

The Crystal Structure of N43D Demonstrates the Structural Basis for Decreased Stability. To explore the structural basis for the decrease in stability observed with N43D, we crystallized the N34LC28 construct containing the N43D mutation and compared it to the wild-type structure, 1SZT (*24*). Figure 4 shows the hydrogen bonding network among Asn-43, Glu-137, and Gln-141 that is present in the wild-type structure. The side chain amide of Asn-43 forms a hydrogen bond with the side chain oxygen of Gln-141 (2.8 Å) and with the side chain oxygen of Glu-137 (3.0 Å). Glu-137 also forms an ion pair (3.0 Å) with Arg-46 from HR1 (not shown). In other structures of the six-helix bundle, Gln-141 is rotated away from Asn-43 and the Asn-43 side chain makes hydrogen bonds with Glu-137 and the side chain of Gln-39 of HR1 (*33*). We have determined structures of

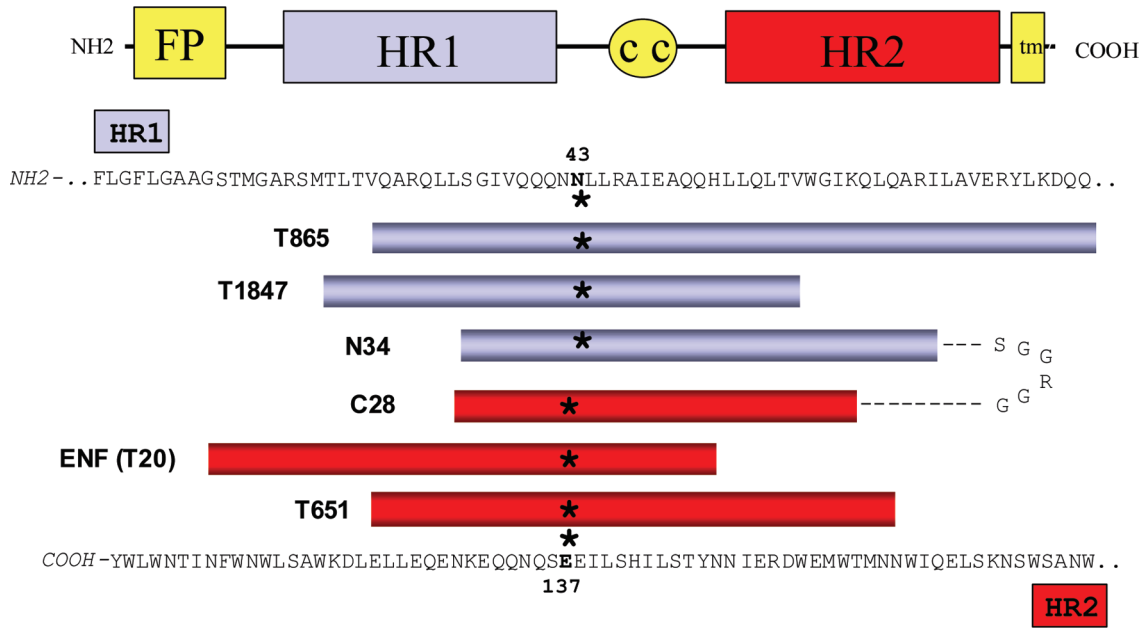

FIGURE 2: Sequence of HR1 and HR2 peptides used in this study, which corresponds to the sequence of the laboratory-adapted III_B strain. The HR2 region is shown antiparallel to HR1 to highlight the sequence overlap, and the location of Asn-43 (Asn-554) and Glu-137 (Glu-648) in each peptide construct is denoted with asterisks. The approximate overlap of HR1 and HR2 is based on the crystallographic structure of the six-helix bundle (*21*).

Table 2: Helicity and Thermal Stability of HR1−HR2 Complexes As Measured by Circular Dichroism

	% helicity (sum/mix)		T_m (°C)		
peptide complex	pH 7, 10 + 10 μM	pH 3, 1 + 1 μM	pH 7, 10 + 10 μM	pH 3, 1 + 1 μM	pH 7, 8 M urea (1 + 1 μM)
T-1847−T-20	14/90	28/78	47	43	−
T-1847(N43D)−T-20	9/26	26/75	nd[a]	41	−
T-1847−T-20(E137K)	16/ppt[b]	26/86	ppt[b]	40	−
T-1847(N43D)−T-20(E137K)	11/49	25/72	33	37	−
	pH 7, 1 + 1 μM	pH 3, 1 + 1 μM	pH 7, 1 + 1 μM	pH 3, 1 + 1 μM	pH 7, 8 M urea (1 + 1 μM)
T-865	74	76	73	71	nd[a]
T-865−T-651	54/84	57/79	86	85	68
T-865(N43D)−T-651	52/81	54/74	73	83	44
T-865−T-651(E137K)	56/86	58/81	87	83	70
T-865(N43D)−T-651(E137K)	54/82	55/71	79	82	53
N34LC28 WT	−	−	70	−	−
N34LC28 N43D	−	−	61	−	−
N34LC28 E137K	−	−	72	−	−
N34LC28 N43D/E137K	−	−	70	−	−

[a] No apparent transition was observed. [b] Precipitation was observed.

several WT and mutant bundles, and both of these configurations have been observed.

The crystal structure of the N43D mutant indicates that the backbones of the HR1 and HR2 helices are very similar to that of the wild type at positions away from the N43D mutation (rms deviation of the superposition of 0.81 Å). Figure 5 shows the superposition of the wild-type structure with the N43D mutant at the site of the mutation. The presence of Asp-43 has a profound effect on the structure of the six-helix bundle. Strikingly, the hydrogen bond network that is present in the wild-type structure is completely destroyed, and HR2 undergoes a local unwinding, which moves Gln-141 and Gln-142 away from HR1. The last five residues of HR2, or approximately one turn of helix, are no longer helical.

In addition to the loss of HR2 contact, the N43D mutation places a negative charge 2.6 Å from Glu-137. This results in a repulsive electrostatic interaction between these two residues. Interestingly, the backbone of the HR1 helix is slightly displaced at the site of the mutation, and this movement acts to increase the distance between Asp-43 and Glu-137. It is possible that the defect observed in the HR1 helix is due to these repulsive interactions, but it is also possible that it is a result of the large changes in the HR1−HR2 interface in this region. Arg-46, which originally formed an ion pair with Glu-137, now forms a salt bridge with Asp-43 (not shown). However, a sulfate ion is also present near Arg-46 in the mutant structure and may influence the position of this side chain.

N43D Is Less Deleterious in N45LC36. Since Asn-43 is positioned eight amino acids from the N-terminus of the N34LC28 construct, we were concerned that this chimera may not be the most appropriate for studying this mutation. Also, since the C-terminal end of the HR2 peptide lies near the site of the mutation, structural changes may be exaggerated by end effects. Therefore, we sought to determine

Table 3: Crystallographic Statistics for Structures of N43D

	N43D	N45LC36 N43D	N45LC36 N43D/E137K
	Data Collection		
space group	*R*3	$P2_13$	$P2_13$
cell dimensions			
a, *b*, *c* (Å)	51.02, 51.02, 59.69	59.52, 59.52, 59.52	59.29, 59.29, 59.29
α, *β*, *γ* (deg)	90, 90, 120	90, 90, 90	90, 90, 90
resolution (Å)	17.76−1.56	50.0−1.95	50.0−2.10
R_{merge} (%)	3.5	8.9	9.6
$I/\sigma I$	30.9	8.0	9.3
completeness (%)	84.7	91.8	91.2
	Refinement		
resolution (Å)	1.8	2.0	2.1
no. of reflections	34304	4548	3876
R_{work}/R_{free}	23.4/25.8	24.9/28.6	24.2/31.8
no. of atoms			
protein	546	607	607
ligand/ion	0	0	0
water	15	22	29
B-factor			
protein	33.81	45.02	60.82
water	39.91	53.07	62.48
root-mean-square deviation			
bond lengths (Å)	0.005	0.004	0.005
bond angles (deg)	0.87	0.77	0.83

the crystal structure of a longer HR1−HR2 chimera containing N43D. Finding an appropriate length for both HR1 and HR2 that would permit solubilization and crystallization proved to be challenging, but we were successful with a chimera containing 45 HR1 residues and 36 HR2 residues (N45LC36). The complete description of the design and structure of this construct will be presented elsewhere (Z. Wang, D. Ahrens, X. Bai, and J. J. Dwyer, unpublished observations), but this construct represents the longest peptide model of the six-helix bundle crystallized to date and provides a better venue for studying the impact of resistance mutation within the region of residues 36−45.

Interestingly, when the structure of the N45LC36 chimera with the N43D mutation was determined, we found that the structural perturbation introduced by Asp-43 was much less significant than in the shorter construct. Unlike the N36LC28 N43D structure, the HR2 helix does not unwind. Furthermore, instead of a close-range, unfavorable electrostatic interaction with Glu-137, there is a solvent-mediated hydrogen bond network involving Asp-43, Glu-137, Gln-39, and HOH-96 (Figure 6A). This general geometry is observed in the wild-type N45LC36 structure (Z. Wang, D. Ahrens, X. Bai, and J. J. Dwyer, unpublished observations). Although the longer bundles were found to have extremely high thermal stability, the T_m of N45LC36 N43D is only a few degrees lower than that of wild-type N45LC36 (not shown).

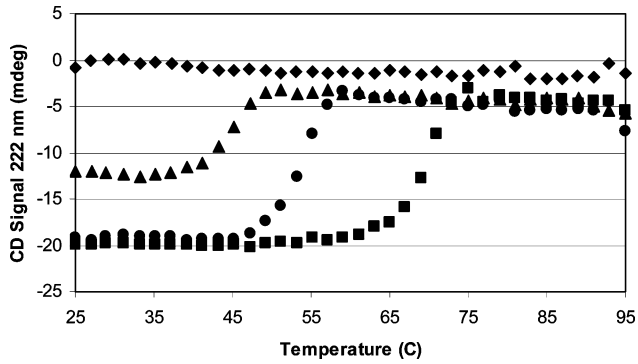

FIGURE 3: Thermal stability of HR1−HR2 bundles as determined by circular dichroism. Equal amounts of HR1 and HR2 (1 *μ*M each) were mixed and melted in PBS and 8 M urea (pH 7.0). Thermal unfolding transitions (monitored at 222 nm) for complexes of T-651 and T-865 (■) and T-865 analogues containing the N43D (▲) and N43D/E137K (●) substitutions. The HR1 peptide T-865 (◆) is unstructured under these conditions, as is T-651 (not shown).

We were also able to crystallize the N43D/E137K double mutant in the longer construct. The local environment around the N43D/E137K mutation (Figure 6B) indicates that the two residues are within ion pairing distance (4.4 Å). Interestingly, the water molecule is present in the double mutant as well and forms hydrogen bonds with both Asp-43 and Lys-137.

DISCUSSION

The development of novel antiviral agents that can achieve durable virologic suppression in patients with viruses resistant to existing therapies remains an ongoing challenge. Since ENF is the first fusion inhibitor to be approved for clinical use, it is important to understand the mechanism by which such resistance mutations affect ENF sensitivity and impact viral fitness and pathogenesis. Recent studies demonstrating that patients who develop resistance to ENF may still derive immunological benefit upon continued ENF therapy (*13*) highlight the unusual mechanistic properties of these mutations. Furthermore, understanding the mechanism by which ENF resistance mutations impact viral fusogenicity may help develop novel fusion inhibitors with enhanced activity against resistant virus. In this work, we have explored the structural impact of a common ENF resistance mutation, N43D, and a related polymorphism, E137K.

ENF resistance mutations have been shown to decrease the sensitivity of viruses to the peptide, and this decrease in activity is associated with a reduction in the binding affinity of the peptide (*10*). The N43D mutation has been shown to reduce the stability of the six-helix bundle, and the crystal structure of the N34LC28 N43D mutant reveals that this mutation causes a significant disruption in the interaction between the HR2 peptide and the HR1 target. Specifically, the helicity of the HR2 peptide in the bound state is decreased by an unwinding of the final turn of helix on the C-terminal end of the peptide. The reduction in stability and the loss of helical structure are due primarily to altered electrostatic interactions rather than to changes in hydrophobic contact at the HR1−HR2 interface. In particular, at least two hydrogen bonds between HR1 and HR2 are broken in response to the mutation, and a repulsive charge−charge interaction between Asp-43 and Glu-137 is present which likely further reduces stability. These changes no doubt influence the binding affinity of ENF or other HR2 peptides that bind in this area and provide a structural basis for the loss of ENF activity. In addition, ENF resistance mutations have been shown to enhance viral sensitivity to neutralizing antibodies, suggesting an enhanced exposure of some epitopes (*12, 22*). If the N43D mutation alters the structural presentation of the fusion intermediate state or increases the time that epitopes are exposed, these changes may provide a basis for the increased sensitivity to neutralizing antibodies.

An unexpected finding was the differential impact of N43D in the N45LC36 chimera. In this longer construct, N43D was found to have much less impact on stability and helical

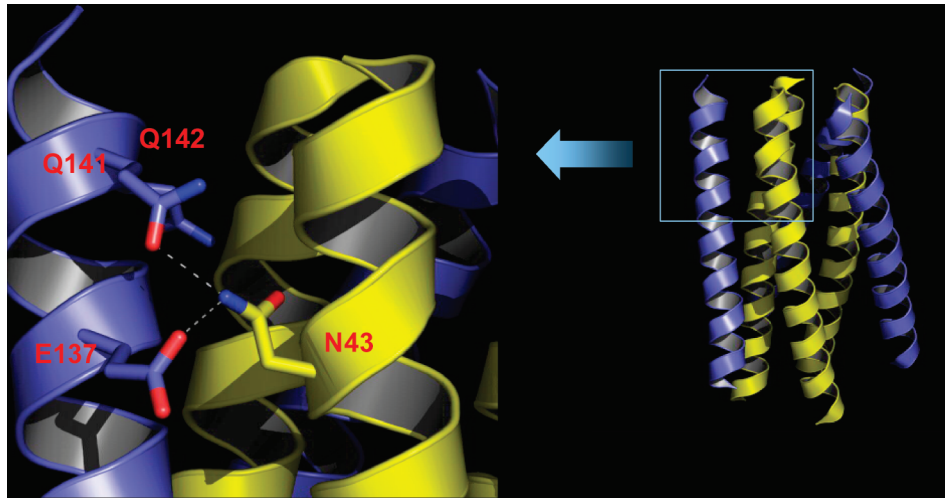

FIGURE 4: Hydrogen bonding interactions between Asn-43 and HR2 amino acids Glu-137 and Gln-141 in the N34LC28 wild-type structure (*24*). HR1 is colored yellow and HR2 blue. All figures were prepared using PyMOL (*35*).

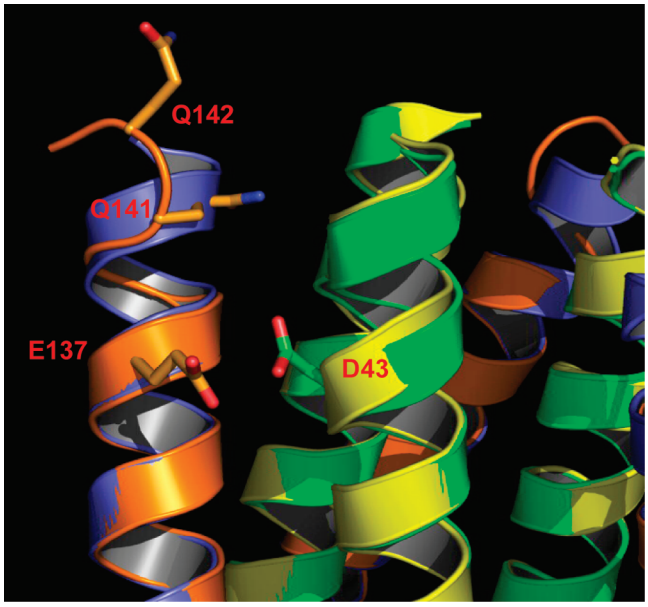

FIGURE 5: Superposition of the N34LC28 N43D mutant structure (HR1 in green and HR2 in orange) with the wild-type bundle. The unstructured C-terminal end of HR2 in the mutant structure is depicted as a wire; however, the electron density in this region was not clearly defined.

structure. This difference appears to be the result of a solvent molecule that bridges several key contact residues at the interface of HR1 and HR2. In the shorter construct, the OE1 atom of Gln-141 is placed at approximately the same position as the water molecule in the longer chimera. It is unclear whether this difference is due to the length of the peptides or to the crystallization conditions. However, the similarity in the thermal stability of WT and N43D in the N45LC36 construct suggests that even in standard buffers, the impact of Asp-43 is reduced. If this difference is a result of the increased length of the six-helix bundle, it may suggest that some resistance mutations may be differentially better tolerated in the context of gp41. That is, a mutation that significantly impacts the binding of a short HR2 peptide to the viral HR1 may not have the same impact on the formation of the viral six-helix bundle. Interestingly, T-651 retains full potency against viruses with N43D (J. J. Dwyer, D. K. Davison, and M. L. Greenberg, unpublished observations), despite the reduction of bundle stability reported here. The observed differences in hydrogen bonding patterns between the two constructs and the apparent contributions by solvent molecules around Asn-43 in the longer construct make it difficult to ascertain what might represent an accurate model of viral gp41.

Since ENF and other fusion inhibitor peptides are derived from the viral HR2 region of gp41, it stands to reason that resistance mutations in response to fusion inhibitors may impair viral fitness and pathogenicity by interfering with the formation or stability of the viral six-helix bundle. The HR1 region of gp41 is highly conserved, and mutational analysis has shown that even relatively conservative mutations can lead to significant functional defects (*19–23*). Therefore, the resistance mutations that are selected under drug pressure most likely represent a balance between reduction of ENF sensitivity and maintenance of sufficient fusogenicity to remain viable. Recently, it has been shown that certain mutations do decrease the replicative capacity of the virus in vitro (*11*) and in vivo (*36*), but there is very little understanding of how structural changes in gp41 affect viral fitness or pathogenicity. Viral solutions that are selected in vivo will also be dependent on the genetic background of the virus population (*34*). The interaction between Asp-43 and Lys-137 described in this work represents a detailed description of the influence of specific HR2 residues on the selection of particular resistance mutations in HR1. Such relationships are also evident in the appearance of secondary or compensatory mutations, and we are currently exploring the structural and thermodynamic characteristics of these mutations. It will be interesting to look at other measures of viral function, such as viral entry or fusion kinetics, to more fully explore the functional consequences of N43D. A recent study examined the impact of N43D on viral infectivity in a single-round pseudotype reporter assay and found that viral infectivity was decreased by 92% by this mutation, and this defect in viral entry or fusion was alleviated by the E137K polymorphism (*18*). These results support our assertion that N43D confers substantial fitness defects to HIV-1, and these defects may be largely eliminated by the E137K polymorphism/compensatory change.

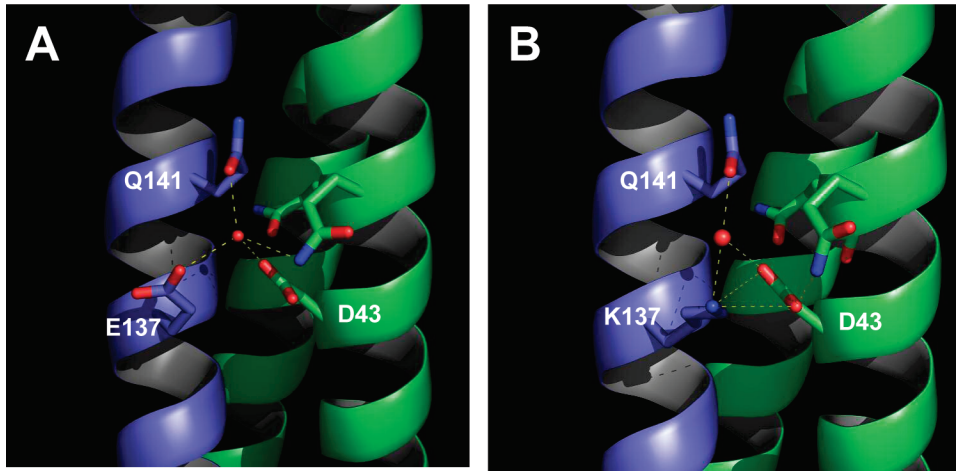

FIGURE 6: Impact of N43D (A) and N43D/E137K (B) mutations on the structure of N45LC36. Hydrogen bonds to a localized solvent molecule are indicated.

Although the structures presented here may not be fully reflective of the viral six-helix bundle, changes in the helical HR1 backbone or the rearrangement in HR2 may provide a framework for understanding the structural basis of changes in fitness or pathogenesis in response to N43D. This work also provides a path forward for the development of novel fusion inhibitor peptides that have activity against viruses containing the N43D mutation. For example, in the recently described class of helix-stabilized peptides (*26*), the amino acid corresponding to Glu-137 is substituted with alanine. Therefore, this mutation should have a much weaker effect on the activity of these peptides, and preliminary data have confirmed this (J. J. Dwyer, D. K. Davison, and M. L. Greenberg, unpublished observations). It also suggests that longer HR2 peptides may have improved potency and durability if they are able to bind to a mutated gp41 without significant loss of helical structure.

An interesting finding in this work was the frequency of emergence of N43D in the presence of strains containing Lys-137 at baseline, which suggests that N43D alone may be highly deleterious to the virus. A recent study demonstrated that E137K was able to partially restore the infectivity lost in a virus containing the N43D mutation (*18*), which supports a function reason why these mutations may occur together. The change in ENF susceptibility conferred by N43D or N43D/E137K is similar, so Lys-137 appears to have little direct impact on ENF susceptibility. Biophysical analysis suggests that Lys-137 forms an ion pair with Asp-43 and that this interaction stabilizes the bundle. The crystal structure of the N43D/E137K double mutant also supports the ion pair hypothesis, although the ion pair geometry is not ideal.

In summary, the crystal structure of a six-helix bundle containing the common ENF resistance mutation, N43D, has provided a detailed molecular model for the loss of ENF sensitivity and the decrease in bundle stability. The defects observed in response to N34LC28 N43D demonstrate that a single mutation in gp41 can lead to dramatic changes in the HR1−HR2 interface. Studying the impact of other resistance mutations on the structure and stability of the six-helix bundle should further clarify the mechanism by which ENF sensitivity is lost. Coupled with functional data, it will also form a mechanistic framework for understanding how these mutations alter viral function and pathogenesis in vivo and may aid in the development of novel fusion inhibitors targeting HIV or other infectious agents.

ACKNOWLEDGMENT

We thank Dr. Hengmin Ke of the University of North Carolina (Chapel Hill, NC) for assistance with the crystal structure of N34LC28 N43D and Dr. Mary Dwyer of Duke University for help in preparing the structure figures. We also thank Peter Jeffs and Dani Bolognesi for their support of this work.

REFERENCES

1. Wild, C., Oas, T., McDanal, C., Bolognesi, D., and Matthews, T. (1992) A synthetic peptide inhibitor of human immunodeficiency virus replication: Correlation between solution structure and viral inhibition. *Proc. Natl. Acad. Sci. U.S.A. 89*, 10537–10541.
2. Wild, C. T., Shugars, D. C., Greenwell, T. K., McDanal, C. B., and Matthews, T. J. (1994) Peptides corresponding to a predictive α-helical domain of human immunodeficiency virus type 1 gp41 are potent inhibitors of virus infection. *Proc. Natl. Acad. Sci. U.S.A. 91*, 9770–9774.
3. Rimsky, L. T., Shugars, D. C., and Matthews, T. J. (1998) Determinants of human immunodeficiency virus type 1 resistance to gp41-derived inhibitory peptides. *J. Virol. 72*, 986–993.
4. Derdeyn, C. A., Decker, J. M., Sfakianos, J. N., Zhang, Z., O'Brien, W. A., Ratner, L., Shaw, G. M., and Hunter, E. (2001) Sensitivity of human immunodeficiency virus type 1 to fusion inhibitors targeted to the gp41 first heptad repeat involves distinct regions of gp41 and is consistently modulated by gp120 interactions with the coreceptor. *J. Virol. 75*, 8605–8614.
5. Greenberg, M. L., and Cammack, N. (2004) Resistance to enfuvirtide, the first HIV fusion inhibitor. *J. Antimicrob. Chemother. 54*, 333–340.
6. Sista, P. R., Melby, T., Davison, D., Jin, L., Mosier, S., Mink, M., Nelson, E. L., DeMasi, R., Cammack, N., Salgo, M. P., Matthews, T. J., and Greenberg, M. L. (2004) Characterization of determinants of genotypic and phenotypic resistance to enfuvirtide in baseline and on-treatment HIV-1 isolates. *AIDS 18*, 1787–1794.
7. Menzo, S., Castagna, A., Monachetti, A., Hasson, H., Danise, A., Carini, E., Bagnarelli, P., Lazzarin, A., and Clementi, M. (2004) Genotype and phenotype patterns of human immunodeficiency virus type 1 resistance to enfuvirtide during long-term treatment. *Antimicrob. Agents Chemother. 48*, 3253–3259.
8. Melby, T., Sista, P., DeMasi, R., Kirkland, T., Roberts, N., Salgo, M., Heilek-Snyder, G., Cammack, N., Matthews, T. J., and Greenberg, M. L. (2006) Characterization of envelope glycoprotein gp41 genotype and phenotypic susceptibility to enfuvirtide at baseline and on treatment in the phase III clinical trials TORO-1 and TORO-2. *AIDS Res. Hum. Retroviruses 22*, 375–385.
9. Wei, X., Decker, J. M., Liu, H., Zhang, Z., Arani, R. B., Kilby, J. M., Saag, M. S., Wu, X., Shaw, G. M., and Kappesa, J. C. (2002)

Emergence of resistant human immunodeficiency virus type 1 in patients receiving fusion inhibitor (T-20) monotherapy. *Antimicrob. Agents Chemother. 46*, 1896–1905.

10. Mink, M., Mosier, S. M., Janumpalli, S., Davison, D., Jin, L., Melby, T., Sista, P., Erickson, J., Lambert, D., Stanfield-Oakley, S. A., Salgo, M., Cammack, N., Matthews, T., and Greenberg, M. L. (2005) Impact of human immunodeficiency virus type 1 gp41 amino acid substitutions selected during enfuvirtide treatment on gp41 binding and antiviral potency of enfuvirtide in vitro. *J. Virol. 79*, 12447–12454.
11. Lu, J., Sista, P., Giguel, F., Greenberg, M., and Kuritzkes, D. R. (2004) Relative replicative fitness of human immunodeficiency virus type 1 mutants resistant to enfuvirtide (T-20). *J. Virol. 78*, 4628–4637.
12. Reeves, J. D., Lee, F.-H., Miamidian, J. L., Jabara, C. B., Juntilla, M. M., and Doms, R. W. (2005) Enfuvirtide resistance mutations: Impact on human immunodeficiency virus envelope function, entry inhibitor sensitivity, and virus neutralization. *J. Virol. 79*, 4991–4999.
13. Aquaro, S., D'Arrigo, R., Svicher, V., Di Perri, G., Lo Caputo, S., Visco-Comandini, U., Santoro, M., Bertoli, A., Mazzotta, F., Bonora, S., Tozzi, V., Bellagamba, R., Zaccarelli, M., Narciso, P., Antinori, A., and Perno, C. F. (2006) Specific mutations in HIV-1 gp41 are associated with immunological success in HIV-1-infected patients receiving enfuvirtide treatment. *J. Antimicrob. Chemother. 58*, 714–722.
14. Melby, T., DeSpirito, M., DeMasi, R., Heilek, G., Thommes, J. A., Greenberg, M. L., and Graham, N. (2007) Association between specific enfuvirtide resistance mutations and CD4 cell response during enfuvirtide-based therapy. *AIDS 21*, 2537–2539.
15. Xu, L., Pozniak, A., Wildfire, A., Stanfield-Oakley, S. A., Mosier, S. M., Ratcliffe, D., Workman, J., Joall, A., Myers, R., Smit, E., Cane, P. A., Greenberg, M. L., and Pillay, D. (2005) Emergence and evolution of enfuvirtide resistance following long-term therapy involves heptad repeat 2 mutations within gp41. *Antimicrob. Agents Chemother. 49*, 1113–1119.
16. Cabrera, C., Marfil, S., Garcia, E., Martinez-Picado, J., Bonjoch, A., Bofill, M., Moreno, S., Ribera, E., Domingo, P., Clotet, B., and Ruiz, L. (2006) Genetic evolution of gp41 reveals a highly exclusive relationship between codons 36, 38 and 43 in gp41 under long-term enfuvirtide-containing salvage regimen. *AIDS 20*, 2075–2080.
17. Lalezari, J. P., DeJesus, E., Northfelt, D. W., Richmond, G., Wolfe, P., Haubrich, R., Henry, D., Powderly, W., Becker, S., Thompson, M., Valentine, F., Wright, D., Carlson, M., Riddler, S., Haas, F. F., DeMasi, R., Sista, P. R., Salgo, M., and Delehanty, J. (2003) A controlled Phase II trial assessing three doses of enfuvirtide (T-20) in combination with abacavir, amprenavir, ritonavir and efavirenz in non-nucleoside reverse transcriptase inhibitor-naive HIV-infected adults. *Antiviral Ther. 8*, 279–287.
18. Tolstrup, M., Selzer-Plon, J., Laursen, A. L., Bertelsen, L., Gerstoft, J., Duch, M., Pedersen, F., and Ostergaard, L. (2007) Full fusion competence rescue of the enfuvirtide resistant HIV-1 gp41 genotype (43D) by a prevalent polymorphism (137K). *AIDS 21*, 519–521.
19. Cao, J., Bergeron, L., Helseth, E., Thali, M., Repke, H., and Sodroski, J. (1993) Effects of amino acid changes in the extracellular domain of the human immunodeficiency virus type 1 gp41 envelope glycoprotein. *J. Virol. 67*, 2747–2755.
20. Lu, M., Stoller, M. O., Wang, S., Liu, J., Fagan, M. B., and Nunberg, J. H. (2001) Structural and functional analysis of interhelical interactions in the human immunodeficiency virus type 1 gp41 envelope glycoprotein by alanine-scanning mutagenesis. *J. Virol. 75*, 11146–11156.
21. Weng, Y., and Weiss, C. D. (1998) Mutational analysis of residues in the coiled-coil domain of human immunodeficiency virus type 1 transmembrane protein gp41. *J. Virol. 72*, 9676–9682.
22. Follis, K. E., Larson, S. J., Lu, M., and Nunberg, J. H. (2002) Genetic evidence that interhelical packing interactions in the gp41 core are critical for transition of the human immunodeficiency virus type 1 envelope glycoprotein to the fusion-active state. *J. Virol. 76*, 7356–7362.
23. Suntoke, T. R., and Chan, D. C. (2005) The fusion activity of HIV-1 gp41 depends on interhelical interactions. *J. Biol. Chem. 280*, 19852–19857.
24. Tan, K., Liu, J., Wang, J., Shen, S., and Lu, M. (1997) Atomic structure of a thermostable subdomain of HIV-1 gp41. *Proc. Natl. Acad. Sci. U.S.A. 94*, 12303–12308.
25. Malashkevich, V. N., Chan, D. C., Chutkowski, C. T., and Kim, P. S. (1998) Crystal structure of the simian immunodeficiency virus (SIV) gp41 core: Conserved helical interactions underlie the broad inhibitory activity of gp41 peptides. *Proc. Natl. Acad. Sci. U.S.A. 95*, 9134–9139.
26. Dwyer, J. J., Wilson, K. L., Davison, D., Freel, S. A., Seedorff, J. E., Wring, A. A., Tvermoes, N. A., Matthews, T. J., Greenberg, M. L., and Delmedico, M. K. (2007) Design of helical, oligomeric HIV-1 fusion inhibitor peptides with potent activity against enfuvirtide-resistance virus. *Proc. Natl. Acad. Sci. U.S.A. 104*, 12772–12777.
27. Hu, Q. X., Barry, A. P., Wang, Z. X., Connolly, S. M., Peiper, S. C., and Greenberg, M. L. (2000) Evolution of the human immunodeficiency virus type 1 envelope during infection reveals molecular corollaries of specificity for coreceptor utilization and AIDS pathogenesis. *J. Virol. 74*, 11858–11872.
28. Kimpton, J., and Emerman, M. (1992) Detection of replication-competent and pseudotyped human immunodeficiency virus with a sensitive cell line on the basis of activation of an integrated β-galactosidase gene. *J. Virol. 66*, 2232–2239.
29. Edelhoch, H. (1967) Spectroscopic determination of tryptophan and tyrosine in proteins. *Biochemistry 6*, 1948–1954.
30. Johnson, W. C. (1990) Protein secondary structure and circular dichroism: A practical guide. *Proteins: Struct., Funct., Genet. 7*, 205–214.
31. Dwyer, J. J., Hasan, A., Wilson, K. L., White, J. M., Matthews, T. J., and Delmedico, M. K. (2003) The hydrophobic pocket contributes to the structural stability of the N-terminal coiled coil of HIV gp41 but is not required for six-helix bundle formation. *Biochemistry 42*, 4945–4953.
32. Weissenhorn, W., Dessen, A., Harrison, S. C., Skehel, J. J., and Wiley, D. C. (1997) Atomic structure of the ectodomain from HIV-1 gp41. *Nature 387*, 426–430.
33. Chan, D. C., Fass, D., Berger, J. M., and Kim, P. S. (1997) Core structure of gp41 from the HIV envelope glycoprotein. *Cell 89*, 263–273.
34. Labrosse, B., Morand-Joubert, L., Goubard, A., Rochas, S., Labernardiere, J. L., Pacanowski, J., Meynard, J. L., Hance, A. J., Clavel, F., and Mammano, F. (2006) Role of the envelope genetic context in the development of enfuvirtide resistance in human immunodeficiency virus type 1-infected patients. *J. Virol. 80*, 8807–8819.
35. DeLano, W. L. (2002) The PyMOL Molecular Graphics System, version 0.92, DeLano Scientific, San Carlos, CA.
36. Deeks, S. G., Lu, J., Hoh, R., Neilands, T. B., Beatty, G., Huang, W., Liegler, T., Hunt, P., Martin, J. N., and Kuritzkes, D. R. (2007) Interruption of enfuvirtide in HIV-1 infected adults with incomplete viral suppression on an enfuvirtide-based regimen. *J. Infect. Dis. 195*, 318–321.

BI702509D